Bloch impedance in negative index photonic crystals

Charles Croënne, Nathalie Fabre, Davy P. Gaillot, Olivier Vanbésien, and Didier Lippens
Institut d'Electronique, de Microélectronique et de Nanotechnologie, Université des Sciences et Technologies de Lille, Avenue Poincaré, Boîte Postale 60069, 59652 Villeneuve d'Ascq Cedex, France

(Received 26 September 2007; revised manuscript received 24 January 2008; published 24 March 2008)

The condition of both relative permittivity and permeability equal to −1 in negative index photonic crystals was addressed by the retrieval of the so-called Bloch impedance. The dispersion characteristics of a photonic crystal made of an array of air holes in an InGaAsP semiconductor layer were first compared (i) by solving the eigenvalue problem by plane wave expansion and (ii) by calculating the complex transmission and reflection coefficients for a finite slab. From the latter, the effective refractive index and the Bloch impedance are deduced by using a transfer matrix technique. The criterion of optical index $n=-1$, which is the key condition for the same focus for all angle incidence, is shown to be satisfied at a frequency where $\varepsilon_{eff}\approx-5$ and $\mu_{eff}\approx-0.2$ and thus far from the condition for impedance matching. A dielectriclike mode of the negative index branch pointed out by field mapping explains the impossibility of effective permittivity and permeability matching to −1.

DOI: 10.1103/PhysRevB.77.125333 PACS number(s): 42.70.Qs, 41.20.Jb, 42.25.Gy

I. INTRODUCTION

Negative refraction in negative index materials (NIMs) opens the way to focusing a point source by using a simple slab, as it was demonstrated in the seminal work of Veselago.[1] In addition, the fine details of a source can be restored in its image focused by such a slab owing to the amplification of evanescent waves, overcoming by this way the diffraction limit.[2] This condition of focusing by negative refraction requires an optical index (n) equal to −1 for a material with both effective permittivity (ε_{eff}) and permeability (μ_{eff}) equal to −1.[3] So far, negative refraction as well as imaging with a better resolution than that predicted by the diffraction limit were experimentally demonstrated mainly at microwave frequencies.[4,5] In optics, subwavelength imaging was also shown by using a silver slab,[6] following the proposal of Pendry to focus an image using a layer of metal. Some theoretical and experimental studies also addressed negative refraction in a flat lens by taking benefit of the left-handed dispersion band in photonic crystals (PCs).[7–31] On the theoretical side, the criterion $n=-1$ by using a PC flat lens was pointed out by notably showing the possibility to use the folded second band, which exhibits a left-handed dispersion branch, whereas an insensitivity to the incidence angle was achieved with round-shaped frequency contours in the Brillouin zone.[32]

In contrast, the problem of satisfying the criterion $\varepsilon_{eff}=\mu_{eff}=-1$ was scarcely discussed,[18,33] despite the fact that the matching of waves via the surface impedance appears as one of the key problems for high resolution imaging, optical writing, or nanolithography.

In this paper, special attention was paid to the problem of index ($n=-1$) and impedance ($\varepsilon_{eff}=-1$ and $\mu_{eff}=-1$) matching in an NIM slab constituted by a PC. To this aim, we start from the design of a real flat lens constituted by a hole array in a semiconductor host substrate whose scattering properties were recently studied.[34] The numerical finite-difference time-domain simulations reported in this paper on the focusing via a PC slab showed huge reflection at input and within the slab, which forms a Fabry-Pérot cavity, which is a characteristic of a strong mismatch, as also depicted in Fig. 1, whereas the condition of index matching is met. We explain here the reasons why both conditions are difficult to satisfy with the calculation of the refractive index and of the impedance. For the latter, we consider a bulk impedance in the sense that it is not dependent on a specific interface. Recently, the term of Bloch impedance was proposed for designing the impedance of a metamaterial under such a condition.[35,36] In the following, we will use this wording related to the propagation of Bloch waves. In addition, the dispersion of the effective permittivity and permeability will be deduced from the frequency dependence of the index n and the impedance z.

In order to determine these intrinsic properties of the material and not those related to the interfacing of the slab in a cladding medium, we proceeded in two stages. In the first one, we treated the problem of the calculation of the refractive index in an infinite periodic medium and thus under Bloch wave conditions. We show that the effective parameter n_{eff} describes the propagation of waves within the photonic crystal medium with an airlike mode for the right-handed branch and a dielectriclike mode for the left-handed one. In order to determine the Bloch impedance, in a second stage, we performed the calculation of the complex transmission (T) and reflection (R) coefficients for finite NIM slabs. In order to show that the results are meaningful with insensitivity to the thickness of the slab, various numbers of basic cells were considered along the propagation direction which show similar dispersion characteristics. In a second stage, we applied a Fresnel inversion technique in order to deduce from R and T the two effective parameters $n=\sqrt{\varepsilon_{eff}\mu_{eff}}$ and $z=\sqrt{\mu_{eff}/\varepsilon_{eff}}$, where ε_{eff} and μ_{eff} are the effective permittivity and permeability of the corresponding homogeneous medium, respectively. The effective permittivity ε_{eff} exhibits strong dispersion with values ranging from −40 to 0 at a plasmalike frequency, whereas μ_{eff} does not exceed −0.2 over the left-handed transmission branch.

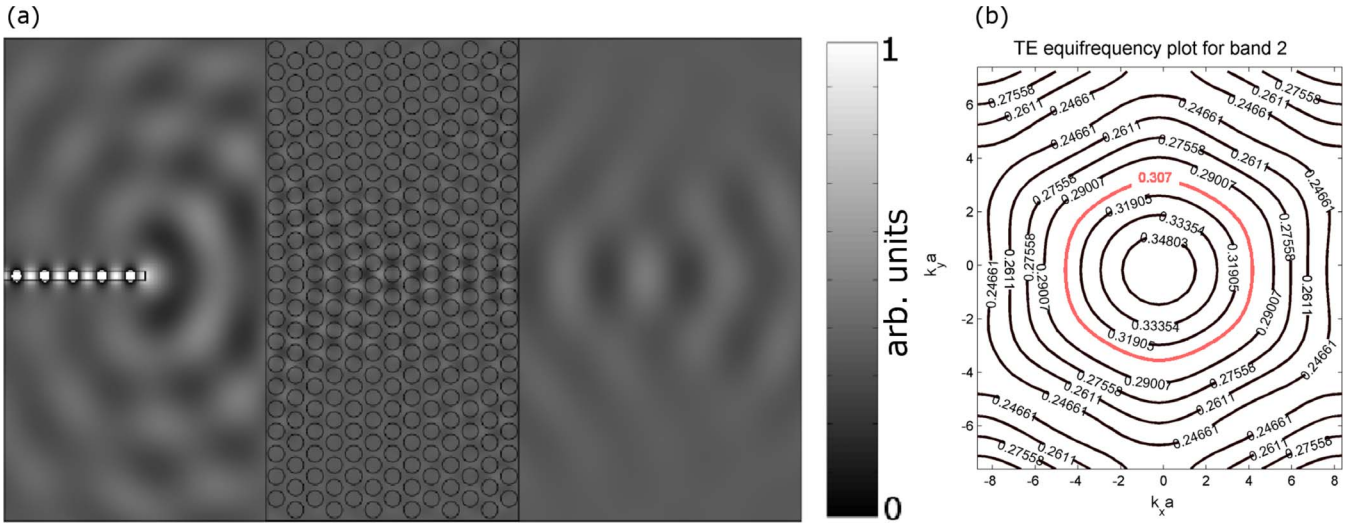

FIG. 1. (Color online) (a) The electric field map (amplitude of the out of plane E component in arbitrary units) obtained by simulation of a 2D photonic crystal showing strong impedance mismatch. (b) The corresponding equifrequency contours in the second band. Since they are round shaped around operation frequency [reduced frequency of 0.307, in red (dark gray)], all angle negative refraction is achieved, with an index value of −1.

II. DETERMINATION OF REFRACTIVE INDEX AND BLOCH IMPEDANCE

The photonic crystal considered in Ref. 33 was made of a trilayered (InP/InGaAsP/InP) semiconductor epilayers in order to achieve a vertical confinement of the electromagnetic wave[37] along the growth direction. In this layer, we patterned on a nanoscale and then etched an air hole array (triangular lattice) in order to tailor the dispersion characteristic of the medium. Here, for the sake of simplicity with respect to the boundary conditions, we assumed a square lattice with a pitch of 450 nm, while the air holes have a diameter of 300 nm. Under these assumptions, the basic cell is constituted of one hole and the effects of the periodicity in the transverse directions and of the truncation in the propagation direction can be modeled according to Fig. 2. Propagation is along the x direction (Γ-X) for an H field polarization along the z direction. In order to consider a two-dimensional (2D) problem, avoiding by these means the three-dimensional full wave analysis, we assumed that the host semiconductor substrate in which the holes are drilled is infinite along the z direction with an effective index $n=3.32$ (relative permittivity of 11). A loss tangent was introduced with the goal to avoid numerical problems faced when the dielectrics losses are set strictly to zero. Finally, it should be emphasized that the structure under test is not clad by air layers inserted between the input and output ports.

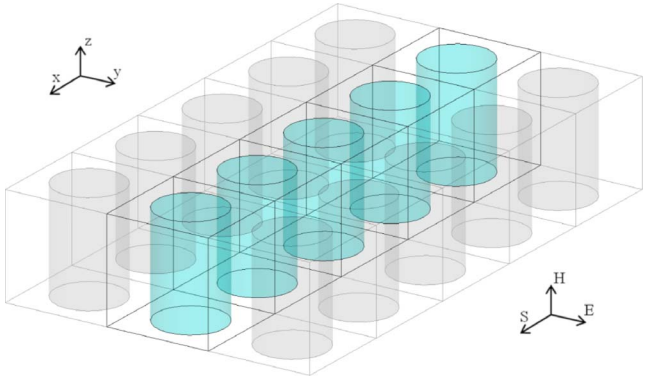

FIG. 2. (Color online) Schematic of the square lattice PC with the relevant directions and incident polarization. The central row is the actual simulation domain, whereas the shaded cells are virtual neighbors introduced by the boundary conditions.

Figure 3(a) shows the results of the calculation of the band structure along the main crystal directions. This dispersion diagram was calculated using the BANDSOLVE code by RSoft based on plane wave expansion. A left-handed dispersion branch ($\vec{v_g}\cdot\vec{v_p}<0$, where $\vec{v_g}=\partial\omega/\partial\vec{k}$ and $\vec{v_p}=\omega/\vec{k}$ are the group and phase velocities, respectively) can be noted between the reduced frequencies ($\mathrm{fr}=\omega a/2\pi c=a/\lambda$) $\mathrm{fr}_1=0.25$ and $\mathrm{fr}_2=0.35$. The light line $n=1$ crosses this left-handed dispersion branch around the reduced frequency $\mathrm{fr}=0.3$ along the Γ-X direction. With $a=450$ nm, this corresponds to the nominal wavelength of the optical telecommunication systems of 1.55 μm, for which the index matching condition is met thus for a PC slab embedded in air.

Figures 3(b) and 3(c) show the H-field maps for the first right-handed dispersion branch and the second left-handed one. It can be seen that the energy is mainly localized in air for the former (airlike dispersion mode), whereas most of the energy is localized in the semiconductor for the latter (dielectriclike mode).

Let us now consider the dispersion characteristics of finite PC slabs along the Γ-X direction and let us vary the number of basic cells along the propagation direction. In order to determine the corresponding dispersion characteristic, we first calculated the complex transmission and reflection characteristics by means of the finite element software HFSS (Ansoft). The output data are the complex scattering matrix

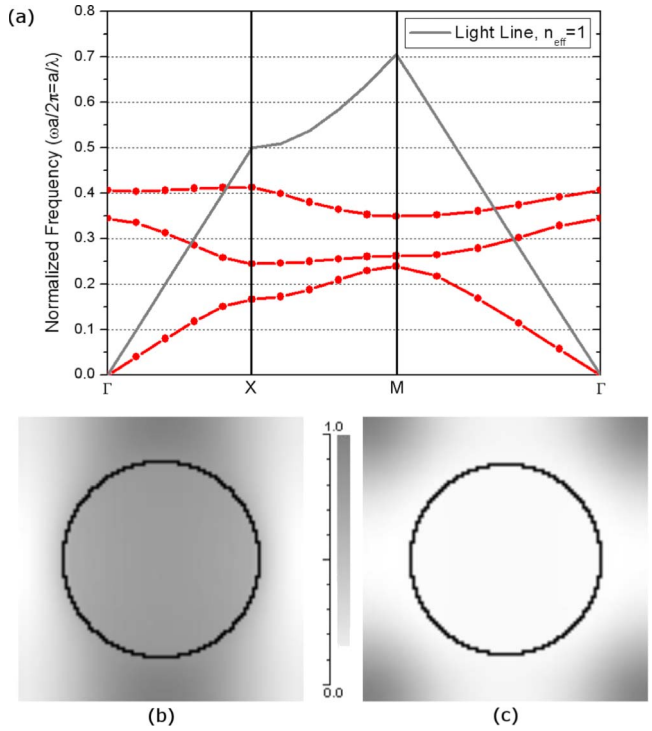

FIG. 3. (Color online) Dispersion band diagram (a) and normalized magnetic field profiles in the (b) first and (c) second bands, calculated under (b) Bloch wave conditions.

whose terms $S_{11}=S_{22}$ depict the reflection coefficient and $S_{12}=S_{21}$ the transmission. The complex transmission and reflection data calculated in the absence of air cladding layers contain the information relative to the real and imaginary parts of the eigenstates of the system.

To determine these complex eigenstates and notably the dispersion characteristics for finite slabs, we convert the scattering matrix S_{ij} into a transfer matrix also called *ABCD* or chain matrix. On the other hand, the chain matrix of a homogeneous propagation medium can be written as a function of a complex propagation constant $\gamma=\alpha+j\beta$, where α and β depict the evanescence of the wave in the forbidden gap and the propagation when we assume a lossless medium. z is the reduced impedance of the propagation medium with respect to its surrounding environment.

$$M=\begin{bmatrix} A & B \\ C & D \end{bmatrix}=\begin{bmatrix} \mathrm{ch}(\gamma a) & z\,\mathrm{sh}(\gamma a) \\ \frac{1}{z}\mathrm{sh}(\gamma a) & \mathrm{ch}(\gamma a) \end{bmatrix}. \quad (1)$$

By equating term by term the various matrix elements of the microstructured and homogeneous media it can be shown that

$$\alpha=\frac{1}{a}\ln|A\pm\sqrt{A^2-1}|, \quad (2)$$

$$\beta a=\angle(A\pm\sqrt{A^2-1})+2k\pi, \quad k\in Z, \quad (3)$$

and

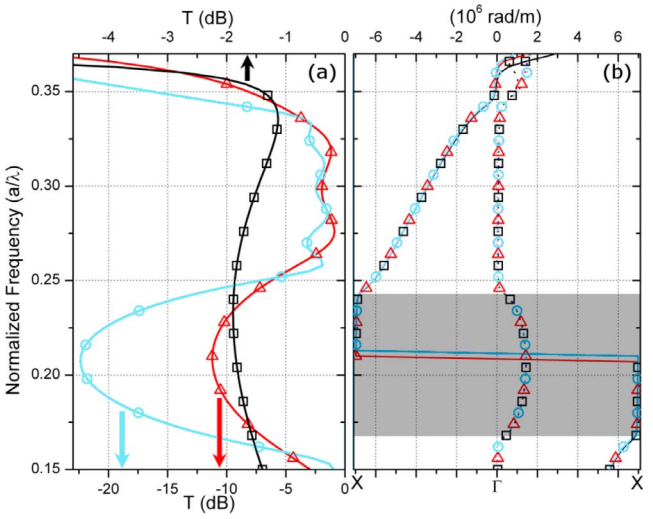

FIG. 4. (Color online) (a) Frequency dependence of the transmission and (b) of α (dotted lines) and β (solid lines) for one (black, □), three [red (dark gray, △)] and five [light blue (light gray, ○)] cells along the Γ-*X* direction. The grayed out frequency band is the first forbidden gap.

$$z=\pm\sqrt{\frac{B}{C}}. \quad (4)$$

The information about the index is present in the complex propagation constant since

$$n=\frac{c\gamma}{i\omega}. \quad (5)$$

This inversion technique is equivalent to the one initially presented by Weir.[38] It has been successfully applied to double negative metal structures such as split ring resonators and wire arrays.[39]

It remains to define the boundary conditions. For the TM polarization considered here, adequate boundary conditions must be applied to the simulation cell. On top and bottom of the simulation domain, we assumed perfect magnetic conductors, while the sidewalls of the modeling box are constituted of perfect electric conductors. At last, we define two ports for the remaining boundaries. One is used to supply a plane wave and to record the wave reflected by the PC slab, whereas the other one probes the scattered waves. Both ports can be considered as matching loads in the sense that any impinging wave crosses the boundaries without reflection. In an experimental situation, this would correspond to an infinite cladding medium.

III. FREQUENCY DEPENDENCE OF THE TRANSMISSION AND REFLECTION

The frequency dependence of the magnitude of the transmission along the Γ-*X* direction is plotted in Fig. 4(a) for one, three, and five cells. As notably expected from frequency filtering theory, the dip in the transmission spectra, which corresponds to the forbidden gap pointed out by the

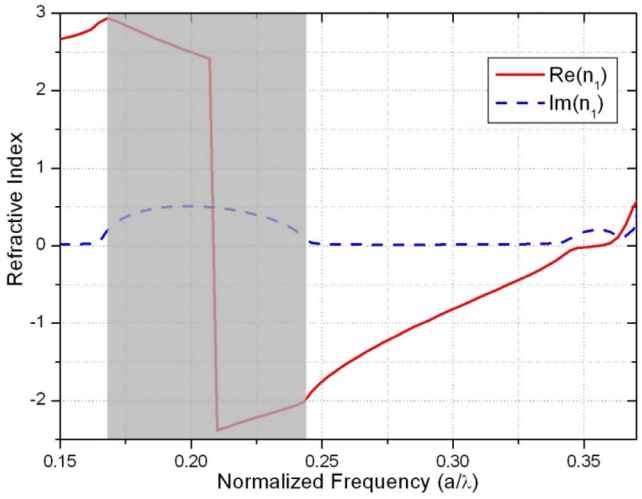

FIG. 5. (Color online) Frequency dependence of the effective complex refractive index along the Γ-*X* direction.

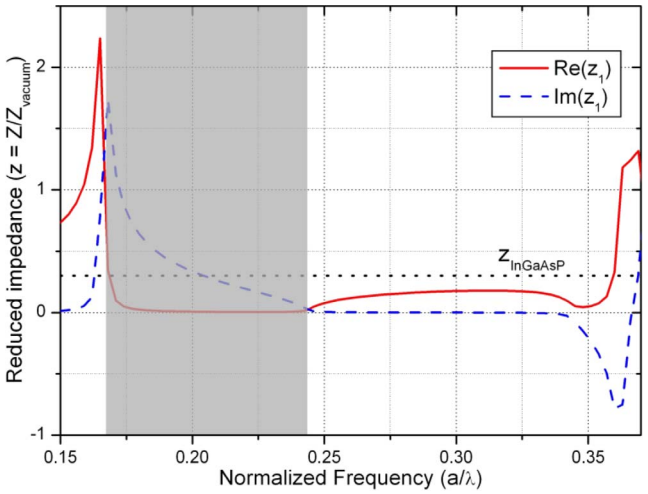

FIG. 6. (Color online) Frequency dependence of the effective complex impedance along the Γ-*X* direction.

band diagram calculation, becomes more and more pronounced when the number of cells is increased. This result is an expected signature of the evanescence of waves since the electromagnetic waves cannot propagate in this frequency gap. Outside this gap, the transmission spectra show different peaks related to the number of cascaded cells.

Figure 4(b) shows the frequency dependence of the real and imaginary parts of the propagation constant times the pitch of the periodic structure a for various numbers of cells between the reduced frequencies of 0.15 and 0.37.

In agreement with the band diagram displayed in Fig. 3(a), a regime of evanescent waves can be noted between fr=0.17 and 0.25. The inversion of band curvature was obtained between 0.25 and 0.35 in agreement with the results shown in Fig. 3(a) for the one-cell prototype β, varying between $-\pi$ and 0. As a consequence v_g is positive, while v_p is negative. Hence, the wave propagation is backward and the refractive index is negative. At this stage, one can conclude that the propagation of waves within the right-handed dispersion band (ground band) and in the left-handed one (second folded band) can be quite accurately described despite the fact that waves propagate over short distances. In order to have more quantitative information, it can be interesting to consider the corresponding refractive index which quantifies the phase shift of the transmitted Bloch waves and the Bloch impedance related to the reflected waves. They are given by Eqs. (4) and (5). At last, it is also possible to formulate the parameters of the effective medium in terms of an effective permittivity and an effective permeability, both complex, given by

$$\varepsilon_{eff} = \frac{n}{z}, \quad \mu_{eff} = nz. \tag{6}$$

It should be emphasized that we do not address the criteria of homogenization. We try to introduce phenomenological parameters which correctly describe the scattering of electromagnetic waves with the nanostructured PCs.

Figure 5 shows the variation versus frequency of the effective refractive index. Its meaning as a parameter which describes the propagation is doubtful in the forbidden gap where high imaginary parts are noted. As a consequence, let us focus on the frequency range of 0.25–0.35 expressed in reduced frequency which corresponds to the backward wave propagation branch. In this branch, n is monotonously increasing from $n=-2$ to $n=0$; this value is achieved around fr=0.35. In the following, this frequency would correspond to a plasmalike frequency where the effective permittivity vanishes. The frequency of index matching is retrieved with a value of reduced frequency close to 0.3. As a last comment, it was found that n is independent of the number of cells for reduced frequencies below 0.35. This corroborates the previous conclusion about the physical meaning of n in truncated geometries. Above fr=0.35, the propagation of wave is multi mode and the retrieval technique is senseless.

Figure 6 is a plot of the frequency variation of the impedance. Within the left-handed dispersion branch, z is real having a low value of the reduced impedance. Note that the value of z for an InGaAsP layer (dashed line) is comparable to the impedance of the microstructure confirming a dielectriclike mode. In contrast, impedance matching was achieved for the right-handed dispersion branch (airlike mode) for a reduced frequency of 0.17. These results show the impossibility to impedance match the PC slab whatever the frequency which is considered in the left-handed dispersion branch.

In Figs. 7 and 8, we plotted the frequency variation of the effective complex permittivity and permeability. For the backward propagation regime, the permittivity, which was found to be independent of the number of cells and in agreement with the previous conclusion, exhibits a Drude-like variation over the left-handed branch with a characteristic plasma frequency at fr=0.37 in the present example. The dynamic of the variation is important: The permittivity takes values as high as −40 at the corner frequency of 0.245. With respect to the ideal case, $\varepsilon_{eff}=-1$ here is achieved at fr =0.35 and thus at the upper frequency edge of the left-handed branch. In contrast, let us recall that the condition

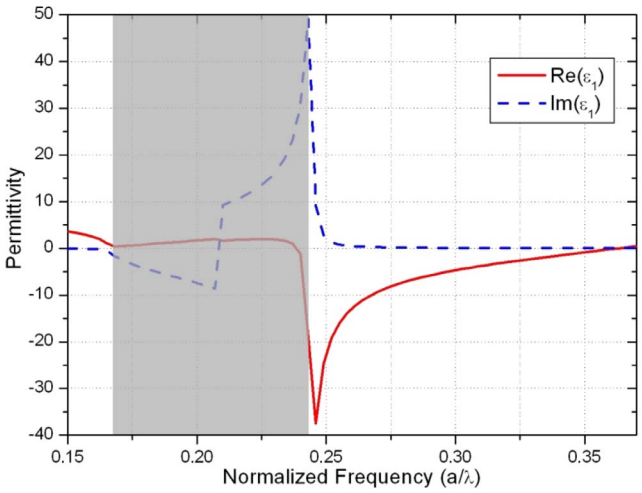

FIG. 7. (Color online) Frequency dependence of the effective complex permittivity along the Γ-*X* direction.

$n=-1$ was obtained at a much lower frequency of 0.28.

The dispersion of the permeability, which is plotted in Fig. 8, shows a magnetic activity. The values are, however, limited to −0.2 and thus never reach the optimal value $\mu_{eff}=-1$ in the frequency band of interest. At the frequency of index matching fr=0.28, the corresponding values of ε_{eff} and μ_{eff} are −5 and −0.2, respectively. Figure 9 presents the 2D field map of the out-of-plane magnetic component for the same PC slab lens presented in Fig. 1 at the frequency of index matching. Here, the surrounding air was modified to have the previously computed impedance while preserving an index of 1. In contrast to Fig. 1, the amount of reflected waves at the air/PC interface is clearly diminished, showing that the computed impedance is relevant. It is noteworthy that the values found here are practically the same as the effective permittivity ($\varepsilon_r=-5.7$) and permeability ($\mu_r=-0.175$) deduced by Decoopman *et al.*[33] Let us recall that the authors of this paper considered the permittivity and permeability of the embedding medium as fitting parameters for

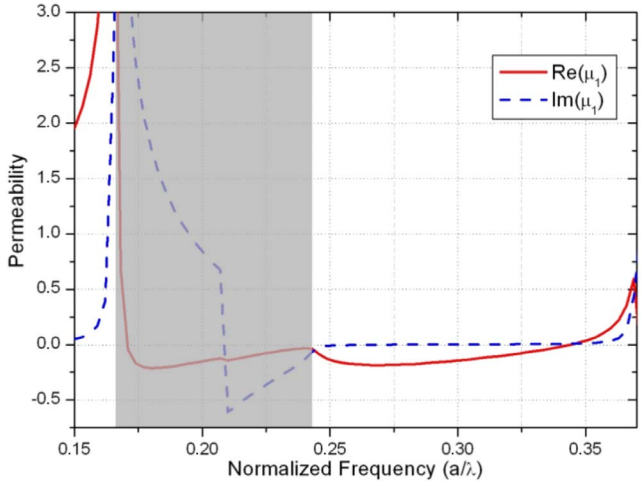

FIG. 8. (Color online) Frequency dependence of the effective complex permeability along the Γ-*X* direction.

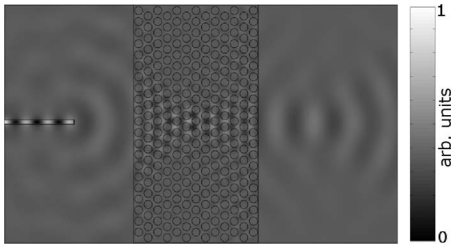

FIG. 9. Example of field map (amplitude of the out of plane *H* component in arbitrary units) obtained by the same simulation as Fig. 1 (same arb. units) of a 2D photonic crystal in a virtual environment with $\varepsilon=5$ and $\mu=0.2$, showing reduced reflection at the PC slab's walls.

minimizing the reflected wave in a focusing experiment of a point source by a flat lens. This also shows that the definition of an impedance with respect to a specific interface as it was performed in Ref. 33 or of a Bloch impedance defined here as a bulk parameter both conclude to the impossibility to match the effective permittivity and permeability to −1 although the condition $n=-1$ can be reached at one frequency.

IV. CONCLUSION

To summarize, we showed that it is possible to determine effective parameters either from the device (phase offset and impedance) or the material point of view (ε_{eff} and μ_{eff}). Here, they give a phenomenological description of the scattering of a plane wave within a photonic crystal slab. This description appears correct in the long wave regime and when the wavelength compares to the relevant dimension as well. The usefulness of such a description is twofold. From the device point of view, it seems incompatible to simultaneously satisfy the condition of index and impedance matching, yielding a strong mismatch at the interface of PC-based flat lenses. This strong mismatch is related to the dielectric mode of the propagation in the left-handed branch. Beyond the demonstration of first principles proofs, this matching is notably of major concern in single refraction (wedge type) devices and double refraction (slab) components. From the physics point of view, it appears that a photonic crystal which exhibits negative refraction resulting from the folding of an upper band into the first Brillouin zone can also be described as a double negative media by taking μ_{eff} and ε_{eff} as the relevant parameters. This should permit one to address other controlling modes of electromagnetic waves in index gradient PCs,[40] in checkerboard devices, and in electromagnetic cloaks.[41]

ACKNOWLEDGMENTS

This work was partly supported by the research program METAPHORE (AC Nanosciences et Nanotechnologies of the French Ministère de la Recherche et des Nouvelles Technologies). C.C. and N.F. would like to thank Delegation Générale pour l'Armement (DGA) and D.P.G. the Institute IRCICA.

[1] V. G. Veselago, Sov. Phys. Usp. **10**, 509 (1968).
[2] J. B. Pendry, Phys. Rev. Lett. **85**, 3966 (2000).
[3] D. Maystre and S. Enoch, J. Opt. Soc. Am. A **21**, 122 (2004).
[4] A. Grbic and G. V. Eleftheriades, Phys. Rev. Lett. **92**, 117403 (2004).
[5] K. Aydin, I. Bulu, and E. Ozbay, Appl. Phys. Lett. **90**, 254102 (2007).
[6] N. Fang, H. Lee, C. Sun, and X. Zhang, Science **308**, 534 (2005).
[7] M. Notomi, Phys. Rev. B **62**, 10696 (2000).
[8] M. Notomi, Opt. Quantum Electron. **34**, 133 (2002).
[9] C. Luo, S. G. Johnson, and J. D. Joannopoulos, Appl. Phys. Lett. **81**, 2352 (2002).
[10] C. Luo, S. G. Johnson, J. D. Joannopoulos, and J. B. Pendry, Phys. Rev. B **65**, 201104(R) (2002).
[11] C. Luo, S. G. Johnson, J. D. Joannopoulos, and J. B. Pendry, Phys. Rev. B **68**, 045115 (2003).
[12] C. Luo, S. G. Johnson, and J. D. Joannopoulos, Opt. Express **11**, 746 (2003).
[13] S. Foteinopoulou and C. M. Soukoulis, Phys. Rev. B **67**, 235107 (2003).
[14] B. C. Gupta and Z. Ye, J. Appl. Phys. **94**, 2173 (2003).
[15] E. Cubukcu, K. Aydin, E. Ozbay, S. Foteinopoulou, and C. M. Soukoulis, Phys. Rev. Lett. **91**, 207401 (2003).
[16] P. V. Parimi, W. T. Lu, P. Vodo, and S. Sridhar, Nature (London) **426**, 404 (2003).
[17] P. V. Parimi, W. T. Lu, P. Vodo, J. Sokoloff, J. S. Derov, and S. Sridhar, Phys. Rev. Lett. **92**, 127401 (2004).
[18] A. L. Efros and A. L. Pokrovsky, Solid State Commun. **129**, 643 (2004).
[19] X. Zhang, Phys. Rev. B **70**, 195110 (2004).
[20] X. Zhang, Phys. Rev. B **70**, 205102 (2004).
[21] A. Berrier, M. Mulot, M. Swillo, M. Qiu, L. Thylén, A. Talneau, and S. Anand, Phys. Rev. Lett. **93**, 073902 (2004).
[22] A. Martinez, H. Miguez, A. Griol, and J. Marti, Phys. Rev. B **69**, 165119 (2004).
[23] R. Gajic, R. Meisels, F. Kuchar, and K. Hingerl, Opt. Express **13**, 8596 (2005).
[24] K. Guven, K. Aydin, K. B. Alici, C. M. Soukoulis, and E. Ozbay, Phys. Rev. B **70**, 205125 (2004).
[25] R. Moussa, S. Foteinopoulou, L. Zhang, G. Tuttle, K. Guven, E. Ozbay, and C. M. Soukoulis, Phys. Rev. B **71**, 085106 (2005).
[26] X. Wang, Z. Ren, and K. Kempa, Opt. Express **12**, 2919 (2004).
[27] S. Foteinopoulou and C. M. Soukoulis, Phys. Rev. B **72**, 165112 (2005).
[28] X. Wang and K. Kempa, Phys. Rev. B **71**, 085101 (2005).
[29] E. Schonbrun, T. Yamashita, W. Park, and C. J. Summers, Phys. Rev. B **73**, 195117 (2006).
[30] T. Matsumoto, K.-S. Eom, and T. Baba, Opt. Lett. **31**, 2786 (2006).
[31] E. Schonbrun, Q. Wu, W. Park, T. Yamashita, C. J. Summers, M. Abashin, and Y. Fainman, Appl. Phys. Lett. **90**, 041113 (2007).
[32] M. Perrin, S. Fasquel, T. Decoopman, X. Mélique, O. Vanbésien, E. Lheurette, and D. Lippens, J. Opt. A, Pure Appl. Opt. **7**, S3 (2005).
[33] T. Decoopman, G. Tayeb, S. Enoch, D. Maystre, and B. Gralak, Phys. Rev. Lett. **97**, 073905 (2006).
[34] N. Fabre, S. Fasquel, C. Legrand, X. Mélique, M. Muller, M. François, O. Vanbésien, and D. Lippens, Opto-Electron. Rev. **14**, 225 (2006).
[35] C. R. Simovski and S. A. Tretyakov, Phys. Rev. B **75**, 195111 (2007).
[36] C. R. Simovski, Metamaterials **1**, 62 (2007).
[37] S. Fasquel, X. Mélique, O. Vanbésien, and D. Lippens, Opt. Commun. **246**, 91 (2005).
[38] W. B. Weir, Proc. IEEE **62**, 33 (1974).
[39] D. R. Smith, S. Schultz, P. Markos, and C. M. Soukoulis, Phys. Rev. B **65**, 195104 (2002).
[40] E. Centeno and D. Cassagne, Opt. Lett. **30**, 2278 (2005).
[41] D. Schurig, J. J. Mock, B. J. Justice, S. A. Cummer, J. B. Pendry, A. F. Starr, and D. R. Smith, Science **314**, 977 (2006).